Available online at www.sciencedirect.com

SciVerse ScienceDirect

journal homepage: www.elsevier.com/locate/jmbbm

Research paper

Structure and micro-computed tomography-based finite element modeling of Toucan beak

Yasuaki Seki[a], *Mason Mackey*[b], *Marc A. Meyers*[a,*]

[a] *Materials Science and Engineering Program, University of California, San Diego, La Jolla, CA 92093, USA*
[b] *National Center for Microscope and Imaging Research Facility, University of California, San Diego, La Jolla, CA 92093, USA*

ARTICLE INFO

Article history:
Received 10 June 2009
Received in revised form
21 July 2011
Accepted 13 August 2011
Published online 5 September 2011

ABSTRACT

Bird beaks are one of the most fascinating sandwich composites in nature. Their design is composed of a keratinous integument and a bony foam core. We evaluated the structure and mechanical properties of a Toucan beak to establish structure–property relationships. We revealed the hierarchical structure of the Toucan beak by microscopy techniques. The integument consists of 50 μm polygonal keratin tiles with ~7.5 nm embedded intermediate filaments. The branched intermediate filaments were visualized by TEM tomography techniques. The bony foam core or trabecular bone is a closed-cell foam, which serves as a stiffener for the beak. The tridimensional foam structure was reconstructed by μ-CT scanning to create a model for the finite element analysis (FEA). The mechanical response of the beak foam including trabeculae and cortical shell was measured in tension and compression. We found that Young's modulus is 3 (S.D. 2.2) GPa for the trabeculae and 0.3 (S.D. 0.2) GPa for the cortical shell. After obtaining the material parameters, the deformation and microscopic failure of foam were calculated by FEA. The calculations agree well with the experimental results.

1. Introduction

Toco Toucan (*Ramphastos toco*) and other avian species like Hornbill have long and thick beaks, primarily used for foraging and fencing activities. In order to tolerate such activities, the beak maintains sufficient rigidity with a light-weight structure. The beak consists of an integument (rhamphotheca) and a closed-cell bony foam. In previous studies, Seki et al. (2005, 2006) have shown that the microscopic structure of the integument consists of overlapping polygonal keratin tiles. The keratin tiles consist of a keratin matrix and 7.5 nm keratin fibers, intermediate filaments IF (Seki et al., 2010). However, the detailed configuration or shape of keratin fibers was still unknown. We used TEM tomography techniques to reveal the arrangement of IF. The rigidity of the beak is mechanically enhanced by the foam core as evidenced by the resistance to buckling of the beak due to the synergism between the integument and the bony foam (Seki et al., 2005). Macroscopically, the mechanical failure of the beak and the beak foam in compression (Seki et al., 2006) and bending (Fecchio et al., 2010) was studied by FEA. The experimental results and FEA exhibited a good agreement in predicting the deformation and failure of beaks. However, the deformation models lack microscopic aspects of mechanical failure of the foam. We have employed μ-CT scanning techniques

* *Corresponding author.* Tel.: +1 858 534 4719; fax: +1 858 534 5698.
E-mail address: mameyers@ucsd.edu (M.A. Meyers).

1751-6161/$ - see front matter © 2011 Elsevier Ltd. All rights reserved.
doi:10.1016/j.jmbbm.2011.08.003

(Borah et al., 2001; Ulrich et al., 1998; Rietbergen et al., 1995; Nagaraja et al., 2004) to microscopically analyze the human trabecular bone through FEA. We utilized these methods to investigate macro to microscopic fracture and deformation of the beak foam.

2. Materials and experimental methods

2.1. Structural analysis

Confocal and scanning electron microscopes, equipped with EDX, were employed for the structural analysis. The operating voltage of SEM was 10–20 kV and the working distance was 8–15 mm. The rhamphotheca (integument) and foam samples were coated with gold–palladium and placed in the environmental scanning electron microscope (FEI Quanta 600) for characterization.

We have prepared TEM samples based on the procedure described by Dresp et al. (2005), Dresp and Langley (2006). The beak keratin was transversely sectioned and soaked in water for 2 h. The specimens were fixed in 2.5% glutaraldehyde in 0.2 M of phosphate buffer saline (PBS) overnight. After rinsing in 1% PBS, the specimens were post-fixed in osmium tetroxide for 5 h. Before the dehydration process, the specimens were soaked in uranyl acetate overnight. Ethanol was used in the dehydration process. The specimens were polymerized and baked in an oven at 50 °C for 48 h. The polymerized specimens were longitudinally and transversely sectioned by ultramicrotome (Reichert-Jung UltracutE) at a thickness of 250 nm. For TEM tomography, the samples were treated with 15 nm gold particles, dried under ambient conditions, and coated with carbon for 20 s. A JEM-4000EF IVEM (400 kV) at the National Center for Microscopy and Imaging Research facility (NCMIR) was used for TEM tomography. Images were taken at every 2° step in a single rotation from −60° to +60°. The set of images was aligned and assembled by IMOD (a software for tomographic reconstruction).

2.2. Mechanical testing

Toco Toucan beaks were sectioned by a jeweler handsaw and knife after natural death of the birds and stored in a desiccator at 50% RH and 20 °C. For the compression testing of the beak foam, we followed the same procedure as the previous compression testing method (Seki et al., 2005). The internal foam core was removed from the beak and was sectioned 13 mm from the extremity of the 16 cm long foam core. The sectioned foam samples were placed in a mechanical testing machine (Instron Model 3342) and compressive loading was applied with a crosshead speed of 1.27 mm/min.

For the tensile testing of the beak trabeculae, we sectioned the trabeculae from the beak foam with a razor blade (length of ~4 mm). The end of trabeculae was affixed in a polymer resin mold that was allowed to harden, and then attached to the fixed end of the machine until the polymer hardened. The trabeculae specimens are typically ~200 μm in diameter and ~1.6 mm in gauge length, which was carefully measured by an optical microscope (Zeiss Axio Imager). After testing, the fracture surface was measured by optical microscopy to estimate the cross sectional area. Twenty-nine trabeculae samples were measured to obtain the mechanical parameters for FEA.

In order to measure the mechanical properties of the trabeculae of the foam in compression, we sectioned the trabeculae from the beak foam using a razor blade. Dimensions of compression samples varied from 2.5 to 4.5 mm in gauge length; 0.09–0.16 mm in thickness; and 0.12–0.28 mm in width. We used superglue to constrain both ends of trabeculae onto metal plates and aligned trabeculae parallel to loading direction. The metal plates were fixed to the Instron Model 3342 machine by double-sided tape. A cross-head speed of 0.05 mm/min was used for the trabeculae. Seventeen trabeculae specimens were measured to obtain the mechanical parameters for FEA.

The bony shell of foam (cortical shell) was tested in tension to take into account the anisotropy between the trabeculae and cortical shell. The cortical shell was carefully sectioned by the razor blade in a rectangular shape and the trabeculae were removed from the shell. The dimensions of the rectangular specimens were: 2 mm in width; 4 mm in length; and 0.15 mm in thickness. The specimen was gripped with the fixture and Instron Model 3342 was used. The cross-head speed of 0.05 mm/min was used for the cortical shell. The mechanical parameters of the cortical shell were used for FEA.

2.3. Finite element method

In order to create an FE model, 150 images scanned at 93 μm resolution by μ-CT (GE explore RS Rodent CT scanner) were used (see Fig. 1). With this resolution, we could capture the main structure of the trabeculae, which contribute to the stiffness of the foam. The CT images were converted to the tri-dimensional structure of the trabeculae and the cortical shell by a marching cube algorithm, shown in Fig. 1. The core part (trabeculae) and shell part (cortical shell) of the beak foam were individually created. The tri-dimensional model of core was created with DDV (Digital Data Viewer) by applying surface mesh. This rough core model was cleaned by removing unnecessary meshes with a special software (Right Hemisphere 5 Deep Exploration CAD Edition and Rhinoceros). The tri-dimensional model of the cortical shell was also created in a similar way. The trabeculae and cortical shell models were meshed with ANSYS ICEM CFD. Finally, we used LS-PrePost to assemble the trabeculae and shell models. All the FEA calculations were carried out by LS-DYNA (Livemore Software Technology, 2007). The model consists of approximately ~36,500 shell elements for the cortical shell and ~672,400 tetrahedron solid elements for the trabeculae. A piecewise linear plasticity model (material model 24) in LS-DYNA was used for the material model. The height of foam model was ~13 mm and the thickness of the cortical shell was taken to be 0.15 mm for FEM calculation.

3. Results

3.1. Hierarchical structure of the Toucan beak

The sandwich structure of the Toucan beak is hierarchically assembled. The maxillary (upper beak) and mandibular beaks

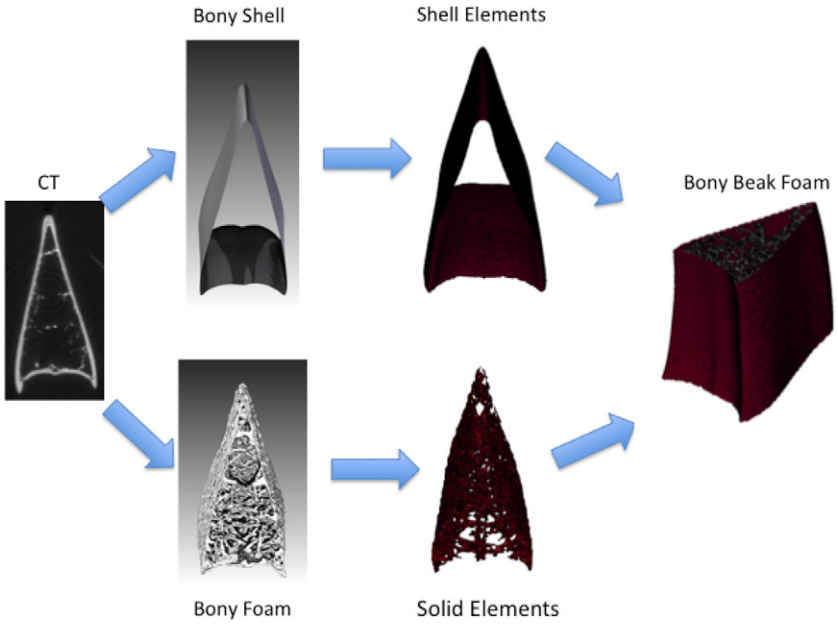

Fig. 1 – Conversion from CT images to the FE model of foam core: 150 CT images were used to create tridimensional models of bony foam and shell by DDV. The models were converted to FE models by ANSYS ICEM CFD. Both models were assembled to make the beak foam core.

(lower beak) are hollow from the proximal end to the midsection, shown in picture and schematics of Fig. 2(a). The Toucan rhamphotheca is ~0.5 mm in thickness whereas the serrations of the beak have the thickness of 1–2 mm. The rhamphotheca has a thickness of ~1 μm and a diameter of 30–60 μm, consisting of polygonal keratin tiles shown in Fig. 2(b). The keratin tile boundaries are wavy, traced by black lines for greater clarity, are shown in the longitudinally sectioned beak keratin in Fig. 2(c). The intermediate filaments are distributed in the keratin matrix, indicated by arrows in Fig. 2(c). The cross sectional mosaic image of lower beak was captured by confocal microscope in Fig. 2(d). The transverse section of the beak keratin exhibits layered structure in Fig. 2(e) and the tiles are connected by an organic glue with an inter-tile spacing of ~18 nm, shown in Fig. 2(f). The intermediate filaments, embedded fibers in the keratin matrix, are either aligned along the cell boundaries or spongy structure in Fig. 2(f). The Toucan beak trabeculae are composed of cylindrical or elliptical rods with ~200 μm in diameter. The porosity of the trabecular bone in beak is enclosed by thin membranes; the typical pore size is 1 mm, Fig. 2(g). This is a different structure from the human trabecular bone, which has no membranes. The average edge connectivity of pores is approximately 3. The trabecular bone is enclosed by a thin cortical shell with a thickness of 150 μm.

3.2. *Structure of IF (intermediate filaments) of beak keratin*

Intermediate Filaments (IF) are so called because their diameter (6–12 nm) is wider than the filaments of myosin and narrower than the filaments of actin. We analyzed the structure of the intermediate filaments (IF) of beak keratin by TEM tomography. The transmission electron micrographs were taken at every 2° angle steps from −60° to 60° with a magnification of 3000. The cell boundaries are drawn by white lines in Fig. 3(a). The IF spread in the keratin tiles and occupy approximately 30% of the tiles. The black dots in the micrographs represent 15 nm of gold particles artificially introduced for imaging, which sometimes agglomerate. The tomogram of the beak keratin was generated from 250 nm thick section (Fig. 3(b)). The IF and boundary of keratin tiles are outlined with the volumetric representation in the tomogram. The tomogram was used to generate a tridimensional structure of IF using the visualization software Amira, shown in Fig. 3(c). The branched structure of IF creates a spongy structure.

3.3. *Mechanical properties of beak trabecular bone*

Fig. 4 shows a typical stress–strain curve of a single trabecula of the Toucan beak. Young's modulus ranges from 0.4 to 7 GPa. The average Young's modulus, obtained from twenty nine measurements, is 3.0 ± (S.D 2.2) GPa. The values reported in the literature have varied from 1 GPa to 19 GPa in tension (Lucchinetti et al., 2000; Bini et al., 2002; Ryan and Williams, 1989; Hernandez et al., 2005). Lucchinetti et al. (2000) discussed the limitations and error sources associated with mechanical testing at the micrometer scale. In order to obtain the strength of the trabeculae, we employed a Weibull distribution. The probability of failure for brittle materials, $F(V)$ is described by

$$F(V) = 1 - \exp\left[-\left(\frac{\sigma}{\sigma_0}\right)^m\right] \quad (1)$$

where σ is the applied stress, σ_0 is the characteristic strength, and m is the Weibull modulus. The characteristic strength is 97 MPa at the failure probability of 63% ($F(V) = 0.63$) and the Weibull modulus is 1.5 for trabeculae, which is typical for brittle materials ($m < 3$).

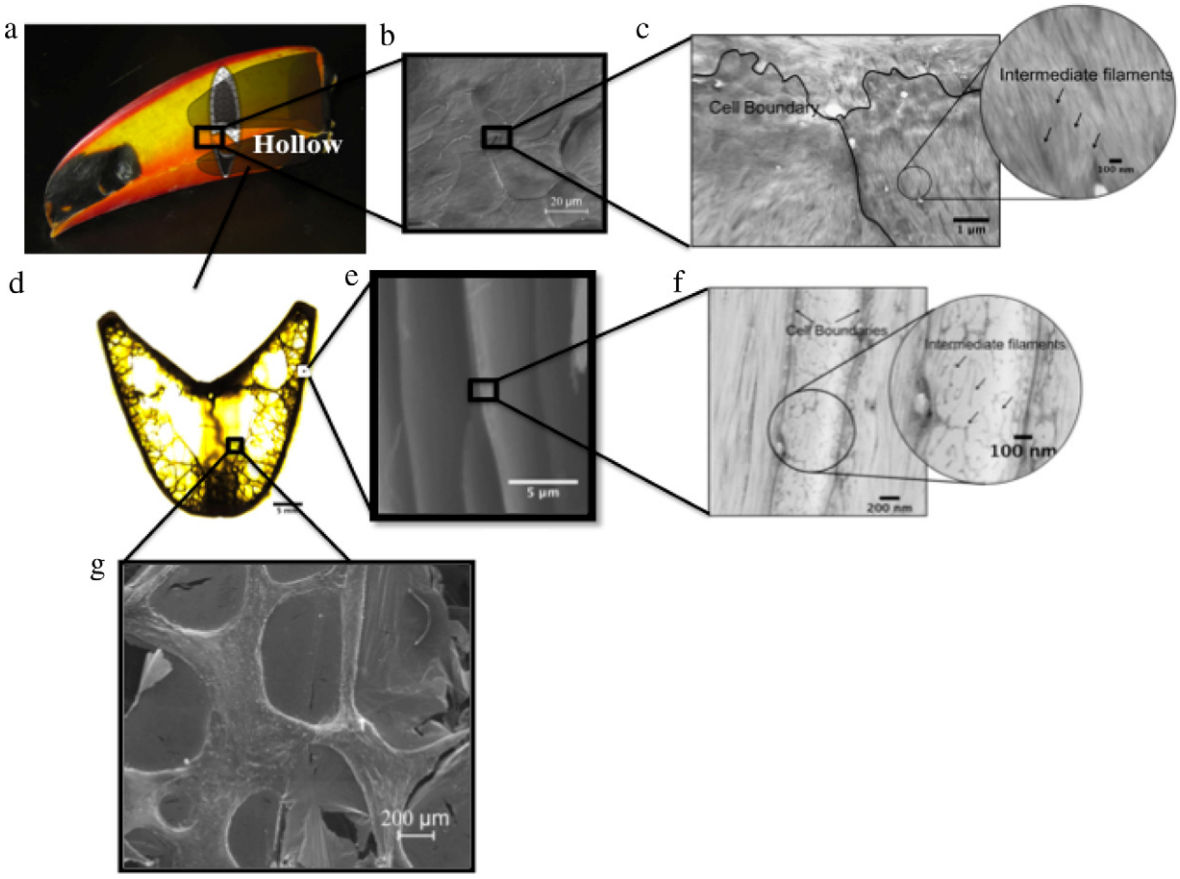

Fig. 2 – Hierarchical structure of the Toucan beak; (a) picture of the Toucan beak, hollow parts are indicated by schematics; (b) surface morphology of beak keratin by SEM; (c) keratin scale structure by TEM, intermediate filaments are indicated by arrows; (d) cross sectional mosaic of lower beak by confocal microscope; (e) cross section of keratin exterior by SEM; (f) TEM of cross section of beak keratin, arrows indicate intermediate filaments; (g) scanning electron micrograph of the foam structure, the cells are sealed by membranes.

We evaluated the mineralization of the tested specimens by EDX. Fig. 5(a) shows the fracture surface of a trabecula with the compositional analysis by EDX. Calcium and phosphorus are homogeneously distributed throughout the trabecula. We investigated the relationship between the calcification and stiffness of the trabeculae. Fig. 5(b) shows Young's modulus plotted as a function of the content of calcium salt. Young's modulus of the trabeculae increases with the degree of calcification. The amount of calcium ranges from 10 to 30 wt%. Young's modulus of trabeculae fluctuates between 1 and 7 GPa.

In most cases, the trabecular bone failed after buckling and bending of the struts. Therefore, we also chose to evaluate the buckling of a single trabecula in compression to obtain the material parameters for the beak foam. The elastic buckling load of a beam is given by the Euler equation:

$$P = \frac{n^2\pi^2 EI}{L^2} \quad (n = 1, 2, 3\ldots) \tag{2}$$

where n is defined by the supports, E is Young's modulus, I is the moment of inertia, and L is the length of beam. If both ends are pinned and fixed, one has $n = 1$ and $n = 2$, respectively.

The corresponding critical stresses σ_{cr} are, for pinned supports and fixed ends:

$$\sigma_{cr} = \frac{\pi^2 E}{(L/r)^2} \quad \text{and} \quad \sigma_{cr} = \frac{4\pi^2 E}{(L/r)^2} \tag{3}$$

where A is the cross sectional area and $r = \sqrt{I/A}$ is the radius of gyration.

The equations for critical stresses are valid for ideal, relatively long columns. In this study, the column slenderness ratio (L/r) is less than 100, which leads to inelastic buckling. Therefore, the tangent modulus theory for inelastic buckling was applied. The corresponding critical stresses for pinned supports and fixed ends are:

$$\sigma_t = \frac{\pi^2 E_t}{(L/r)^2} \quad \text{and} \quad \sigma_t = \frac{4\pi^2 E_t}{(L/r)^2} \tag{4}$$

where E_t is the tangent modulus.

When the slenderness ratio is more than 100, Eq. (4) approach Eq. (3).

Townsend et al. (1975) combined Eqs. (3) and (4) to get

$$\sigma_{cr} = \frac{E_t}{E}\frac{\pi^2 E}{(L/r)^2} \quad \text{and} \quad \sigma_{cr} = \frac{4E_t}{E}\frac{\pi^2 E}{(L/r)^2}. \tag{5}$$

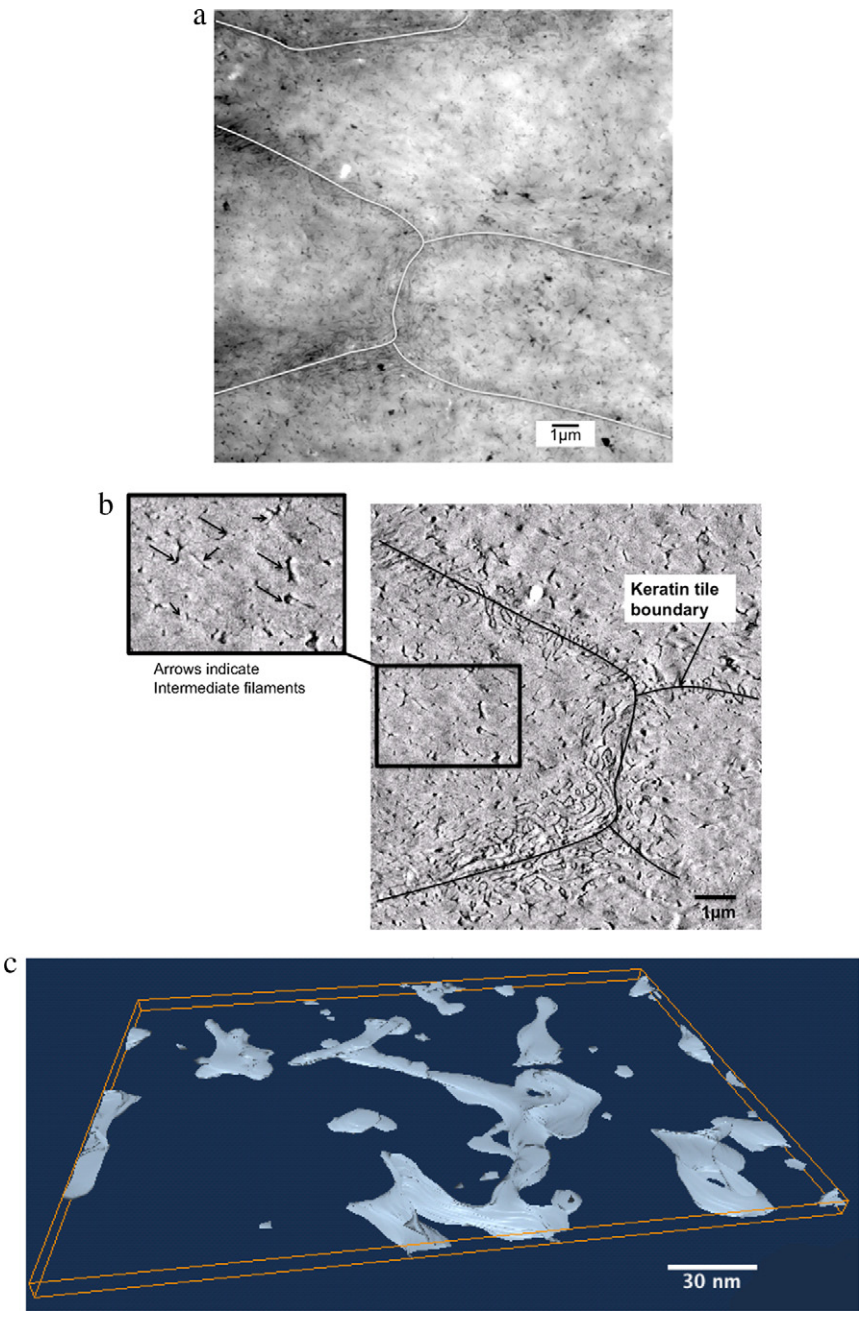

Fig. 3 – (a) TEM image of beak keratin; (b) tomogram of beak keratin, arrows indicate intermediate filaments; (c) tridimensional structure of intermediate filaments (processed by the visualization software Amira).

Fig. 6 shows the two Euler curves with predicted values for pinned and fixed ends trace experimental results. We used Young's modulus of 3 GPa from tensile testing to draw Euler curves. It is simple to envisage that the supports can undergo damage in the assembly of the test setup. If the ends are cracked, a fixed support becomes essentially pinned. The Euler curve for pinned ends tracks the lower buckling stresses and that for fixed ends represents the upper bound for the buckling stresses, Fig. 6. The Euler equation suggests that the estimated Young's modulus matches the assumed 3 GPa value used for elastic buckling.

The cortical shell of the bony beak core was tested in tension in three directions: longitudinal, transverse, and 45°. Young's moduli of cortical shell range from 0.20–0.65 GPa and the tensile strength varies from 5 to 21 MPa. Thus, there is a considerable anisotropy. The stiffness and strength of the cortical bone are substantially lower than those for the trabecular bone. In the case of human bone (Rho et al., 1993; Turner et al., 1999), Young's modulus of the trabecular bone is significantly lower than that of the human cortical bone.

3.4. *FEM modeling of beak trabecular bone*

The experimentally-obtained material parameters of the trabeculae and cortical bone were used for the FEM calculations listed in Table 1. We assumed yield stresses of

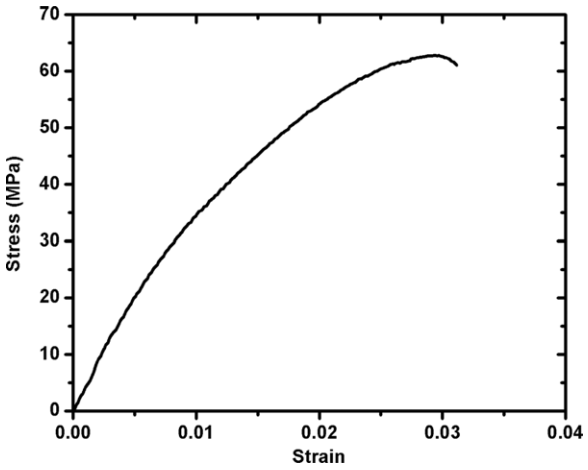

Fig. 4 – Typical stress–strain curve of beak trabecula in tension.

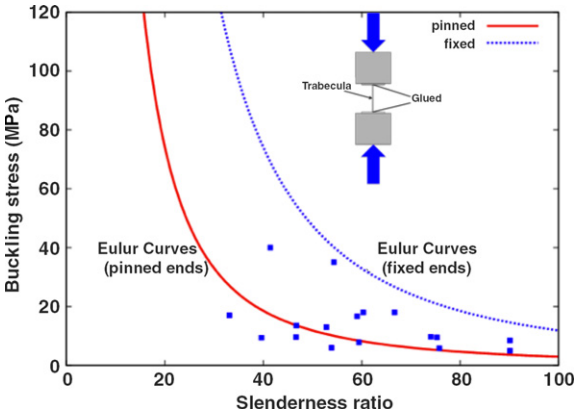

Fig. 6 – Calculated Euler curves of beak trabeculae with fixed ends (dashed curve) and pinned ends (continuous curve) and experimental compressive test results (squares).

σ_y = 20 MPa for trabeculae and σ_y = 10 MPa for the cortical shell. Young's moduli were taken as 3 GPa for trabeculae and 0.3 GPa for the cortical shell. The trabecular and cortical bone were deemed to have failed at strains of 0.03 and 0.1, respectively.

Fig. 7 shows two experimental stress–strain curves of the compressive behavior of the beak foam and a computationally predicted curve with three FE deformation models at different strains. The two experimental stress–strain curves of foam represent different relative densities, 0.06 (with a lower

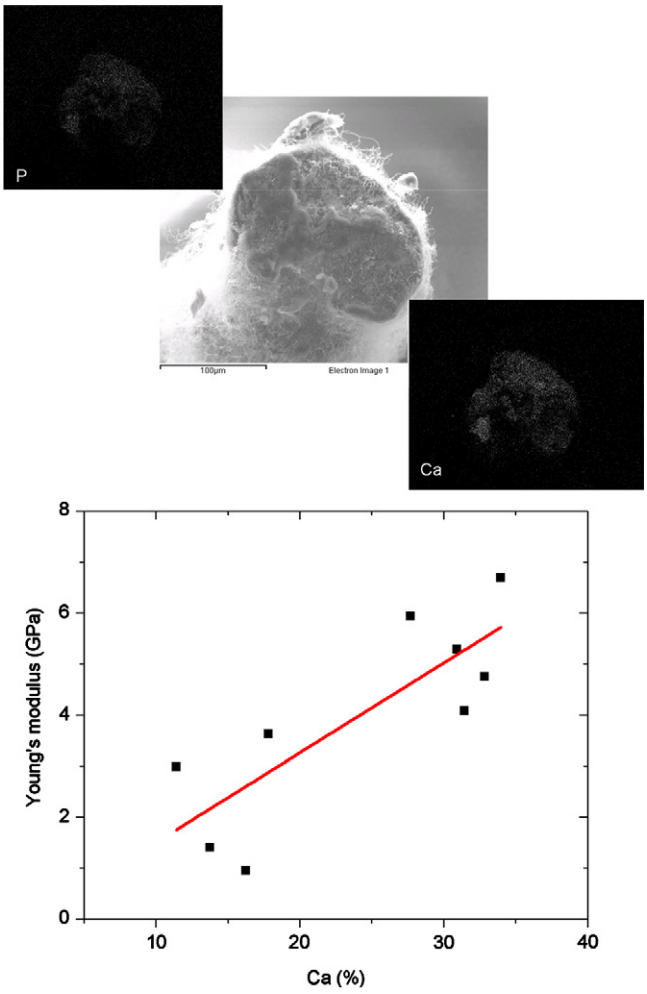

Fig. 5 – (a) Scanning electron micrographs of fracture surface for trabecula subjected to tensile rupture with EDX dot mapping of calcium and phosphorus. (b) Young's modulus vs calcium content (wt%).

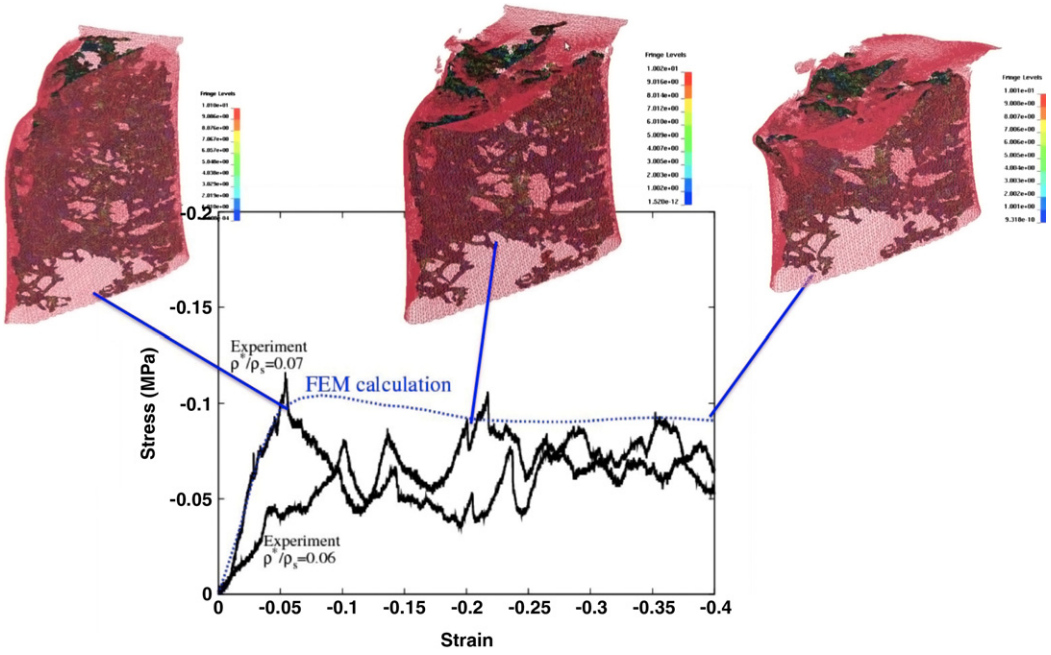

Fig. 7 – Stress–strain curves of beak foam under compression, comparison between experiments and FE calculation. Foams in experiments have relative densities (ρ^*/ρ_S density of foam core/density of foam material) of 0.06 and 0.07.

Table 1 – Mechanical parameters of beak foam for FEA.

	Trabeculae	Cortical shell
Young's modulus	3 GPa	0.3 GPa
Yield stress	20 MPa	10 MPa
Failure strain	0.03	0.1

modulus) and 0.07 (with a higher modulus). The shell folding or buckling is visible at the culmen (upper ridge of a bird beak). At this stage, this deformation is at the end of the linear elastic region. At a strain of −0.20, the trabeculae are compressed and the shell breakage is observed in simulation. The breakage of the shell becomes severe and the trabeculae undergo failure at a strain of −0.40. The calculation shows the average stress at the plateau after the linear elastic region; there is ∼30% difference in the plateau stress and a good agreement in stiffness, in comparison with the experimental stress–strain curve for 0.07 initial relative density.

4. Discussion

The mechanical behavior of bird beaks is governed by both the ductile keratin integument and semi-brittle bony foam. Most of the mechanical loading on the beak is carried by the exterior keratin, whereas the foam increases the energy absorption and stabilizes the deformation of the beak to prevent catastrophic failure (Seki et al., 2005). In the case of the Toucan, the beak is mainly used for apprehension of food so that it is designed to resist bending moments. Indeed, the beak, having hollow core, exhibits a high bending resistance (Seki et al., 2005).

The foam of the Toucan beak is of the closed-cell type unlike other mammalian cancellous bone structures, which are open cell foams. The composition of membranes that seal off the pores constructed by the struts is similar to the trabecular bone, as evidenced through the EDX analysis (Seki et al., 2005). Further investigation is required to verify whether the membranes are part of bone or other materials.

The stiffness of the beak keratin is mechanically isotropic in the transverse and longitudinal directions (Seki et al., 2005). The intermediate filaments (IF) are assumed to be homogeneously distributed in the beak keratin. The IF of beak keratin mechanically play the same role as the fibers for fiber-reinforced composite materials. The branched structure of IF acts as an anchor in the keratin matrix and gives greater strength to the keratin composites. Indeed, the comparison between plain and branched fibers in composites theoretically proves that the branched fiber increases the strength of composites (Shaoyun et al., 1993).

The beak foam is highly mechanically anisotropic due to the anisotropic structure of beak foam. The mechanical testing showed that most values were lower than the human trabecular (Townsend et al., 1975) and cortical bones. The two reasons are the mineralization level and sample handling during the test. The mineralization level is lower than that of the human bone (Seki et al., 2005). As a result, the stiffness is lowered. When we sectioned the samples such as trabeculae and cortical bone, we might have damaged the specimens, which leads to low mechanical properties. In terms of the function of the beak, food gathering does not require a high load bearing capacity, unlike other cancellous bones. This suggests that the beak foam core of the Toucan does not require high stiffness.

5. Conclusions

The Toucan beak is a hierarchically-structured sandwich composite comprised of two materials: keratin and bone.

The structure of the beak keratin consists of polygonal keratin scales that have two constituents: keratin matrix and intermediate filaments. The structure of the intermediate filaments in keratin matrix was successfully identified by TEM tomography and visualization techniques. The intermediate filaments are branched and have a diameter of ~7 nm. The beak foam is composed of trabecular rods with thin membranes that are enclosed by a cortical shell. Macro to microscopic FE modeling of beak foam successfully captured the deformation and failure of the trabeculae and buckling of the cortical shell in compression.

Acknowledgments

We would like to acknowledge the help of Professor David Benson in the implementation of the FEM modeling, Professor Falko Kuester for 3D visualization, and Professor Vlado Lubarda for the help in the mechanistic analysis. We thank Evelyn York at the Scripps Institution of Oceanography (analytical facilities) for assisting with scanning electron microscopy and Professor Robert Mattrey and his scientist Jacqueline Corbeil at Moores Cancer Center at UCSD for CT scan. The TEM analysis was carried out at the National Center for Microscopy and Imaging Research (NCMIR). A special gratitude goes to Sara G. Bodde for the help with experiments. The authors thank the beak provider, Jerry Jennings at the Emerald Forest Bird Gardens. This research was supported by the National Science Foundation, Division of Materials Research, Biomaterials Program (Grant DMR 0510138).

REFERENCES

Bini, F., Marinozzi, A., Marinozzi, F., Patane, F., 2002. Microtensile mesurement of single trabeculae stiffness in human femur. J. Biomech. 35, 1515–1519.

Borah, B., et al., 2001. Three-dimensional microimaging (MRμl and μCT), finite element modeling, and rapid prototyping provide unique insights into bone architecture in osteoporosis. Anat. Rec. 264, 101–110.

Dresp, B., Jouventin, P., Langley, K., 2005. Ultraviolet reflecting photonic microstructures in the King Penguin beak. Biol. Lett. 22, 310–313.

Dresp, B., Langley, K., 2006. Fine structural dependence of ultraviolet reflections in the King Penguin beak horn. Anat. Rec. A 288A, 213–222.

Fecchio, R.S., Seki, Y., Bodde, S.G., Gomes, M.S., Kolososki, J., Rossi, J.L., Gioso, M.A., Meyers, M.A., 2010. Mechanical behavior of prosthesis in Toucan beak (Ramphastos toco). Mater. Sci. Eng., C 30, 460–464.

Hernandez, C., et al., 2005. Trabecular microfracture and the influence of pyridinium and non-enzymatic glycation-mediated collagen cross-links. Bone 37, 825–832.

LS-DYNA Keyword User's Manual. vol. 1. 2007. Livemore Software Technology.

Lucchinetti, E., Thomann, D., Danuser, G., 2000. Review Micromechanical testing of bone trabeculae-potentials and limitations. J. Mater. Sci. 35, 6057–6064.

Nagaraja, S., Couse, T.L., Guldberg, R.E., 2004. Trabecular bone microdamage and microstructural stresses under uniaxial compression. J. Biomech. 38, 707–716.

Rho, J.Y., Ashman, R.B., Turner, C.H., 1993. Young's modulus of trabecular and cortical bone material: ultrasonic and microtensile measurements. J. Biomech. 26, 111–119.

Rietbergen, B.V., Weinans, H., Huiskes, R., Odgaardt, A., 1995. A new method to determine trabecular bone elastic properties and loading using micromechanical finite element models. J. Biomech. 12, 69–81.

Ryan, S.D., Williams, J.L., 1989. Tensile testing of rodlike trabeculae excised from bovine femoral bone. J. Biomech. 22, 351–355.

Seki, Y., Bodde, S.G., Meyers, M.A., 2010. Toucan and hornbill beaks: comparative study. Acta Biomater. 6, 331–343.

Seki, Y., Kad, B., Benson, D.J., Meyers, M.A., 2006. The toucan beak: structure and mechanical response. Mater. Sci. Eng., C 26, 1412–1420.

Seki, Y., Schneider, M.S., Meyers, M.A., 2005. Structure and mechanical behavior of a toucan beak. Acta Mater. 53, 5281–5296.

Shaoyun, F., Wuming, L., Benlian, Z., Chiwei, L., 1993. Theoretical prediction of strength of composite with fractal-tree structure fibers. J. Mater. Sci. Technol. 9, 400–404.

Townsend, P.R., Rose, R.M., Radin, E.L., 1975. Buckling studies of single human trabeculae. J. Biomech. 8, 199–200.

Turner, C.H., Rho, J., Takano, Y., Tusi, T.Y., Pharr, G.M., 1999. The elastic properties of trabecular and cartical bone tissues are similar: results from two microscopic measurement technique. J. Biomech. 32, 437–441.

Ulrich, D., Rietbergen, B.V., Weinans, H., Ruegsegger, P., 1998. Finite element analysis of trabecular bone structure: a comparison of image-based meshing techniques. J. Biomech. 31, 1187–1192.